

Structural Basis for the Function of Stringent Starvation Protein A as a Transcription Factor*

Received for publication, February 7, 2005
Published, JBC Papers in Press, February 25, 2005, DOI 10.1074/jbc.M501444200

Anne-Marie Hansen^{‡§}, Yijun Gu[¶], Mi Li^{**}, Michelle Andrykovitch^{¶‡‡}, David S. Waugh[¶],
Ding Jun Jin^{‡§§}, and Xinhua Ji^{¶¶}

From the [‡]Transcription Control Section, Gene Regulation and Chromosome Biology Laboratory, NCI-Frederick, National Institutes of Health, Frederick, Maryland 21702, the [§]Department of Biochemistry and Molecular Biology, University of Southern Denmark, Campusvej 55, DK-5230 Odense M, Denmark, the [¶]Macromolecular Crystallography Laboratory, NCI-Frederick, National Institutes of Health, Frederick, Maryland 21702, and the ^{**}Basic Research Program, SAIC-Frederick, Frederick, Maryland 21702

Stringent starvation protein A (SspA) of *Escherichia coli* is an RNA polymerase-associated transcriptional activator for the lytic development of phage P1 and is essential for stationary phase-induced acid tolerance of *E. coli*. We report the crystal structure of *Yersinia pestis* SspA, which is 83% identical to *E. coli* SspA in amino acid sequence and is functionally complementary in supporting the lytic growth of phage P1 and acid resistance of an *E. coli* sspA mutant. The structure reveals that SspA assumes the characteristic fold of glutathione S-transferase (GST). However, SspA lacks GST activity and does not bind glutathione. Three regions of SspA are flexible, the N and C termini and the α 2-helix. The structure also reveals a conserved surface-exposed pocket composed of residues from a loop between helices α 3 and α 4. The functional roles of these structural features were investigated by assessing the ability of deletion and site-directed mutants to confer acid resistance of *E. coli* and to activate transcription from a phage P1 late promoter, thereby supporting the lytic growth of phage P1. The results indicate that the flexible regions are not critical for SspA function, whereas the surface pocket is important for both transcriptional activation of the phage P1 late promoter and acid resistance of *E. coli*. The size, shape, and property of the pocket suggest that it mediates protein-protein interactions. SspA orthologs from *Y. pestis*, *Vibrio cholerae*, and *Pseudomonas aeruginosa* are all functional in acid resistance of *E. coli*, whereas only *Y. pestis* SspA supports phage P1 growth.

(RNAP)¹ (1, 2) is a multisubunit enzyme (3) responsible for the transcription process, which consists of initiation, elongation, termination, and recycling steps (for reviews, see Refs. 4–6). One of the major control points is transcription initiation, in which transcription factors modulate the activity of RNAP either positively or negatively at a particular promoter. The *E. coli* stringent starvation protein A (SspA) is an RNAP-associated protein (7) required for the transcriptional activation of phage P1 late genes (8), of which the expression is important for the lytic development of phage P1 (9). Although at present its role in transcription is unknown, SspA is known to be implicated in survival during nutrient starvation and prolonged stationary phase (10). Recently, SspA was shown to play an important role in the stationary phase-induced stress response including acid tolerance by down-regulating the level of the global regulator H-NS (68), which negatively regulates multiple stress defense systems (11, 12). In addition, SspA is highly conserved among Gram-negative bacteria. SspA orthologs in *Neisseria gonorrhoeae*, *Francisella novicida*, *Francisella tularensis*, and *Vibrio cholerae* were shown to affect the expression of genes involved in pathogenesis (13–17).

To gain insight into the structural basis for the function of SspA in transcriptional activation of the phage P1 late promoter and in stationary phase induced acid tolerance of *E. coli*, we determined the three-dimensional structure of SspA. To this end, we cloned, expressed, purified, and characterized SspA from *E. coli*, *Y. pestis*, *V. cholerae*, and *Pseudomonas aeruginosa* (18). All four SspA proteins were subjected to crystallization trials. *E. coli* SspA crystallized but failed to diffract x-rays well enough for structure determination. *P. aeruginosa* SspA also did not form crystals that were suitable for data collection, and *V. cholerae* SspA failed to crystallize under any conditions tested. Only *Y. pestis* SspA crystallized readily, and the crystals diffracted to 2.0 Å. Here, we report the crystal structure of *Y. pestis* SspA, a homologous model of *E. coli* SspA, and the structural basis of *E. coli* SspA function in the development of phage P1 and in stationary phase-induced acid resistance of *E. coli*.

EXPERIMENTAL PROCEDURES

X-ray Diffraction Data Collection and Processing—Crystallization and preliminary x-ray diffraction experiments have been reported else-

Control of transcription is a key step in the regulation of gene expression in all living cells. *Escherichia coli* RNA polymerase

* This work was supported in part with Federal funds from the NCI, National Institutes of Health, under Contract No. NO1-CO-24000. The costs of publication of this article were defrayed in part by the payment of page charges. This article must therefore be hereby marked "advertisement" in accordance with 18 U.S.C. Section 1734 solely to indicate this fact.

The atomic coordinates and structure factors (code 1YY7) have been deposited in the Protein Data Bank, Research Collaboratory for Structural Bioinformatics, Rutgers University, New Brunswick, NJ (<http://www.rcsb.org/>).

¶ Current address: Shanghai Innovative Research Center, 439 Chunxiao Road, Shanghai 201203, China.

‡‡ Current address: Agentase, LLC, 3636 Boulevard of the Allies, Pittsburgh, PA 15213.

§§ To whom correspondence may be addressed: NCI-Frederick, 1050 Boyles St., Bldg. 469, Rm. 127, Frederick, MD 21702-1201. Tel.: 301-846-7684; Fax: 301-846-1456; E-mail: djjin@helix.nih.gov.

¶¶ To whom correspondence may be addressed: NCI-Frederick, 1050 Boyles St., Bldg. 539, Rm. 124, Frederick, MD 21702-1201. Tel.: 301-846-5035; Fax: 301-846-6073; E-mail: jix@ncifcrf.gov.

¹ The abbreviations used are: RNAP, RNA polymerase; PDB, Protein Data Bank; SspA, stringent starvation protein A; MAD, multiwavelength anomalous diffraction; MIR, multiple isomorphous replacement; GSH, glutathione; GST, glutathione S-transferase; GST A1-1, alpha-class GST subunit-type 1; CDNB, 1-chloro-2,4-dinitro-benzene; IPTG, isopropyl-thio- β -D-galactoside; GST S1-1, sigma-class GST subunit type 1; GST B1-1, beta-class GST subunit type 1; r.m.s., root mean square.

TABLE I
Summary of X-ray diffraction data and structure refinement of *Y. pestis* SspA

	Native	Pt-1	Pt-2
Resolution range (Å)	30.0–2.0	30.0–2.8	30.0–2.4
Space group	P6 ₅ 22	P6 ₅ 22	P6 ₅ 22
Cell dimension (Å) ($a = b, c$)	100.4 181.9	100.1 180.2	100.6 183.5
Completeness (%), overall/last shell ^a	99.5/97.4	96.6/92.6	97.6/95.1
Redundancy	7.0	3.4	6.8
$I/\sigma(I)$, overall/last shell	16.1/2.8	7.5/1.9	12.6/3.3
R_{scaling}^b , overall/last shell	0.108/0.519	0.130/0.506	0.103/0.289
Data used for refinement	36,005		
Data used for <i>R</i> -free calculations	1,785		
Final <i>R</i> -factor ^c	0.179		
Final <i>R</i> -free	0.215		
R.m.s. deviations from ideal geometry:			
Bond distances (Å)	0.009		
Bond angles (°)	1.3		

^a 2.02–2.09, 2.90–2.80, 2.40–2.44 Å, for native, Pt-1, and Pt-2, respectively.

^b $R_{\text{scaling}} = \sum |I - \langle I \rangle| / \sigma I$.

^c Crystallographic *R*-factor = $\sum_{\text{hkl}} \|F_o\| - |F_c| / \sum_{\text{hkl}} F_o$.

where (18). The SspA crystals belong to space group P6₅22 (unit cell dimensions $a = b = 100.4$ Å, $c = 181.9$ Å). Native data, at the resolution of 2.0 Å, were collected at the beamline X9B of the National Synchrotron Light Source (Brookhaven National Laboratories) using an ADSC Quantum-4 CCD detector. The Pt-derivative crystal was obtained by soaking native crystals in a solution that was similar to the mother liquor and contained 1.0 mM K₂PtCl₄. The 2.4-Å Pt-derivative data set was collected with an in-house MAR-345 image plate system mounted on a Rigaku rotating anode operated at 50 kV and 100 mA. Multiwavelength anomalous diffraction (MAD) data collection for the Pt-derivative crystal was attempted at the National Synchrotron Light Source. Unfortunately, the crystal diffracted to only 2.8 Å. All crystals were flash frozen and maintained at –173 °C for experiments carried out both in-house and at the synchrotron facilities. The crystallization mother liquor plus 10% MPD was used as the cryoprotectant for data collection. The raw data were processed with Denzo and Scalepack (19). Further data processing was performed with the CCP4 package (20). X-ray data statistics are summarized in Table I.

Crystal Structure Determination—Several phasing options were explored, including MAD phasing at 2.8 Å, single isomorphous replacement with anomalous scattering at 2.4 Å, and multiple isomorphous replacement (MIR) using both 2.4- and 2.8-Å Pt-derivative data sets. SOLVE (21) was used in all phasing trials; the MIR approach resulted in the best electron density map. Four common Pt sites were identified in both Pt derivatives. Additionally, two minor sites were located in each derivative. The heavy atom sites were then refined with SHARP (22), and the phases were improved with DM (23) and Solomon (24). ARP/WARP (25) was used to refine and extend the phases to 2.0 Å and to build the initial model, which contained 389 out of 426 residues. Multiple rounds of refinement were performed using CNS (26) with 5.0% of the data reserved for cross-validation. As the refinement progressed, more residues were located and built into the model and water molecules were identified as peaks in the $F_o - F_c$ electron density map equal to or higher than 3.0 σ . The refinement was coupled with bulk solvent correction. Model building was carried out with O (27). The final model contains 410 amino acids, 441 water molecules, and 2 citrate ions. The average B factor for all atoms is 25.2 Å². The quality of the structure was assessed using PROCHECK (28). A total of 93.4% of the main chain torsion angles are in most favored regions and none in disallowed regions. The refinement statistics can be found in Table I.

Molecular Modeling—The crystal structure of *Y. pestis* SspA was used for the construction of an initial model of *E. coli* SspA. Water molecules in the *Y. pestis* structure were excluded. A monomer of *E. coli* SspA was built with the mutation facility embedded in O (27). Then a dimer of *E. coli* SspA was generated by mimicking the dimeric *Y. pestis* protein. The dimer was subjected to geometry optimization using the conjugate gradient method of Powell (29) embedded in CNS (30). The geometric parameters of Engh and Huber (31) were used as the basis of the force field.

Glutathione Binding Test—The SspA crystals were soaked in a solution that was similar to the crystallization mother liquor and contained 1–5 mM glutathione (GSH) or *S*-hexyl-GSH for 6–24 h before they were frozen for data collection at the National Synchrotron Light Source. Details of data acquisition were as described above. For refinement, the final structure of *Y. pestis* SspA was used as the starting

model. For each data set, one round of refinement using simulated annealing (30) was followed by Difference Fourier synthesis using CNS (26). Visual inspection of the resulting electron density maps was performed with O (27). Neither GSH nor *S*-hexyl-GSH was identified in the structures; therefore, no further refinement was pursued.

BLAST Searches and Multiple Amino Acid Sequence Alignment—BLAST searches were performed to identify orthologs of SspA in genomic sequences available on GenBank™ sites of the National Center for Biotechnology Information (www.ncbi.nlm.nih.gov/) using the tBLASTn program with Blosom 62 matrix; Gap penalties were set at 11 (Existence) and 1 (Extension). In addition, genome data on *Vibrio fischeri* were obtained from the website www.integratedgenomics.com. The multiple sequence alignment was done using ClustalW (32) with a Blosom 30 matrix (gap opening penalty 10 and gap extension penalty 0.05) and refined manually using the GeneDoc program (www.psc.edu/biomed/genedoc, Ref. 33).

Measurement of Glutathione *S*-Transferase Activity—The glutathione *S*-transferase (GST) activity of *Y. pestis* SspA, *E. coli* SspA, RpoS, and alpha-class GST subunit-type 1 (GST A1-1) (PanVera) was measured as their ability to catalyze the conjugation of 1-chloro-2,4-dinitrobenzene (CDNB) to GSH using a GST Detection Module (Amersham Biosciences) according to the manufacturer's instructions. Specific GST activity was calculated as $\mu\text{mol}^{-1} \text{min}^{-1} \text{mg protein}^{-1}$.

Bacterial Strains, Plasmids, Media, and Techniques—Bacterial strains used in this study were derivatives of *E. coli* K12 strain MG1655. Bacterial media, agar plates, and techniques were carried out as described (34). Standard DNA techniques, agar plates and liquid media were used as described (35). Restriction endonucleases (New England Biolabs, Beverly, MA) and the Expand High Fidelity PCR System (Roche Applied Science) used to amplify DNA by PCR, were used according to the manufacturer's instructions.

Deletions and Site-directed Mutagenesis of *E. coli* sspA—Open reading frames encoding N- and C-terminal deletion mutants of SspA, SspAΔ1–9, and SspAΔ204–212, were cloned under the control of an arabinose inducible promoter in pBAD24 (36), resulting in plasmids pDJ602 and pDJ603, respectively.

pDJ602 (pBAD_{ssspA}Δ1–9): A DNA fragment encoding a 27-bp 5'-end deletion of *ssspA* was cloned into the EcoRI/HindIII sites of pBAD24. The DNA fragment was PCR-amplified from MG1655 chromosomal DNA using the oligos *ssspA*Δ1–9 (5'-CAGGACGAATTCACCATGGTAATGACGCTGTTTTCCGGTCT-3') and *ssspA*Δ204–212 (5'-CAGGACAAAGCTTAACCGCCAGACGC-3').

pDJ603 (pBAD_{ssspA}Δ204–212): A DNA fragment encoding a 27-bp 3'-end deletion of *ssspA* was cloned into the EcoRI/HindIII sites of pBAD24. The DNA fragment was PCR-amplified from MG1655 chromosomal DNA using the oligos *ssspA*Δ204–212 (5'-TAGCAGAATTCACCATGGCTGTCGCTGCCAACAAACGTTTCG-3') and *ssspA*Δ1–9 (5'-CAGGACGAATTCACCATGGTAATGACGCTGTTTTCCGGTCT-3').

The following mutants were generated by site-directed mutagenesis of *ssspA* encoded by pDJ600 (68): SspAR82A (pDJ604), SspAP84A (pDJ605), SspAH85A (pDJ606), SspAP86A (pDJ607), SspAY92A (pDJ609), SspAH85A/Y92A (pDJ610), and SspAP84A/H85A/P86A (pDJ611). Site-directed mutagenesis of *ssspA* was carried out using the QuikChange II site-directed mutagenesis kit (Stratagene) as recommended by the manufacturer.

pQE_{ssp}AR82A (pDJ604): Mutagenesis of *sspA* resulting in the amino acid substitution R82A was performed using oligos *ssp*AR82AFW (5'-GAATATCTGGATGAGGCTTCCCGCATCCGCCACTG-3') and *ssp*AR82ABW (5'-CAGTGGCGGATGCGGGAAAGCCTCATCCAGATATTC-3').

pQE_{ssp}AP84A (pDJ605): Mutagenesis of *sspA* resulting in the amino acid substitution R82A was performed using oligos *ssp*AP84AFW1 (5'-TATCTGGATGAGCGTTTCGCGCATCCGCCACTGATGCCTGTT-3') and *ssp*AP84ABW1 (5'-AACAGGCATCAGTGGCGGATGCGCGAAACGCTCATCCAGATA-3').

pQE_{ssp}AH85A (pDJ606): Mutagenesis of *sspA* resulting in the amino acid substitution H85A was performed using oligos *ssp*AH85AFW (5'-CTGGATGAGCGTTTCCCGGCTCCGCCACTGATGCCT-3') and *ssp*AH85ABW (5'-AGGCATCAGTGGCGGAGCCGGAAACGCTCATCCAG-3').

pQE_{ssp}AP86A (pDJ607): Mutagenesis of *sspA* resulting in the amino acid substitution P86A was performed using oligos *ssp*AP86AFW (5'-GATGAGCGTTTCCCGCATCCGCCACTGATGCCTGTT-3') and *ssp*AP86ABW (5'-AACAGGCATCAGTGGCGCATGCGGAAACGCTCATC-3').

pQE_{ssp}AY92A (pDJ609): Mutagenesis of *sspA* resulting in the amino acid substitution Y92A was performed using oligos *ssp*AY92AFW (5'-CTGATGCCTGTTGCCCGGTAGCTCGCGGTGAA-3') and *ssp*AY92ABW (5'-TTCACCGCGAGCTACCGGGCAACAGGCATCAG-3').

pQE_{ssp}AH85A/Y92A (pDJ610): Mutagenesis of *sspA* resulting in substitutions of H85A and Y92 with alanine was performed on pDJ606 using oligos *ssp*AY92AFW and *ssp*AY92ABW.

pQE_{ssp}AP84A/H85A/P86A (pDJ611): Mutagenesis of *sspA* resulting in substitutions of P84A, H85A, and P86A was performed using oligos *ssp*AP84A/H85A/P86AFW (5'-GGAATATCTGGATGAGCGTTTCGCGGCTGCGCCACTGATGCCTGT-3') and *ssp*AP84A/H85A/P86ABW (5'-ACAGGCATCAGTGGCGCAGCCGCGAAACGCTCATCCAGATATTCC-3').

Mutant pQE_{ssp}ABP84A/H85A/P86A (pDJ612) were generated by site-directed mutagenesis of *sspA* encoded by pDJ706. Mutagenesis of *sspA* resulting in substitution of P84A, H85A, and P86A was performed using oligos *ssp*AP84A/H85A/P86AFW and *ssp*AP84A/H85A/P86ABW.

Cloning of *Y. pestis* *sspA*, *V. cholerae* *sspA*, and *P. aeruginosa* *sspA*—The constructs pBAD_{ssp}AYp (pDJ613), pBAD_{ssp}AVc (pDJ614), and pBAD_{ssp}APa (pDJ615) encode *Y. pestis* *sspA*, *V. cholerae* *sspA*, and *P. aeruginosa* *sspA*, respectively, under the control of an arabinose inducible promoter in pBAD24.

pBAD_{ssp}AYp (pDJ613): A DNA fragment encoding *Y. pestis* *sspA* was PCR-amplified from pRIL_{ssp}AYp (18) using the oligos YpVc_{ssp}AUS1 (5'-CCATCGGAATTCACCATGGCTGTGCTG CCAACAACGT-3') and Yp_{ssp}ADS (5'-TTTCTAAGCTTTAGCTCCGAGTTTTCAGATG-3') and cloned into the EcoRI/HindIII sites of pBAD24.

pBAD_{ssp}AVc (pDJ614): A DNA fragment encoding *V. cholerae* *sspA* was PCR amplified from pRIL_{ssp}AVc (18) using the oligos YpVc_{ssp}AUS1 (5'-TAGCAGGGATCCATGGCTGTGCTGCCAACAACGT-3') and Vc_{ssp}ADS (5'-TTTACTAAGCTTTAGCTGCGAGCCAGCAGCACTCTC-3') and cloned into the EcoRI/HindIII sites of pBAD24.

pBAD_{ssp}APa (pDJ615): A DNA fragment encoding *P. aeruginosa* *sspA* was PCR-amplified from pRIL_{ssp}APa (18) using the oligos PasspAUS1 (5'-CCATCGGAATTCACCATGGCTTCAATCAACAAGCTGACC-3') and PasspADS (5'-TTTACTAAGCTTTAGCTCCGAGTTTTCAGATG-3') and cloned into the EcoRI/HindIII sites of pBAD24.

Acid Resistance Test—The acid resistance test was performed as described previously (68). Overnight cultures (18 h) grown in LB at 37 °C were diluted 1:1000 in warm LB, adjusted to pH 2.5 with HCl (6 N), and incubated for 2 h at 37 °C. The number of colony forming units per milliliter was determined by plating serial dilutions of cells in phosphate-buffered saline (pH 7.4) on LB agar plates before and after exposure to acid. The LB agar plates were incubated overnight at 37 °C. Acid survival was calculated as the percentage of cells remaining after acid treatment compared with the initial number of cells. Each experiment was repeated independently at least three times.

The ability of *E. coli* wild-type and mutant SspA proteins, as well as the *Y. pestis*, *V. cholerae*, and *P. aeruginosa* SspA proteins to complement stationary phase acid intolerance of the *sspA* mutant strain DJ6000 (68) was determined by expressing *sspA* *in trans* from plasmids. The *E. coli* wild-type (pQE_{ssp}A) (pDJ600) (68)) and the site-directed mutant *sspA* genes (pQE_{ssp}AR82A, pQE_{ssp}AH85A, pQE_{ssp}AP86A, pQE_{ssp}AY92A, and pQE_{ssp}AP84A/H85A/P86A) were expressed from a *tac* promoter in the absence of the inducer isopropyl-thio- β -D-galactoside (IPTG). The *E. coli* *sspA* deletion mutants (pBAD_{ssp}A1–9 and

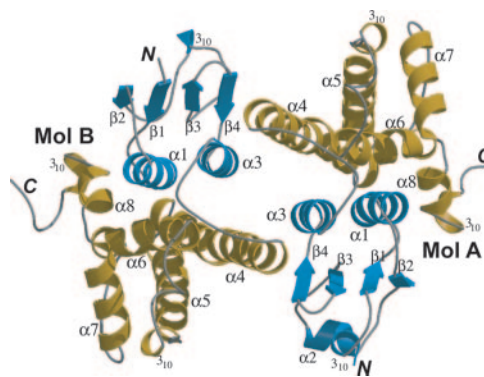


FIG. 1. Overall structure of *Y. pestis* SspA. The dimeric molecule is illustrated as *ribbon diagrams* (helices as *spirals*, β -strands as *arrows*, and loops as *pipes*) with the two domains of each subunit colored in *cyan* and *orange*, respectively. The figure was prepared with MOLSCRIPT (65) and Raster3D (66).

pBAD_{ssp}A Δ 204–212), as well as the wild-type genes from *E. coli* (pBAD_{ssp}ABEc (pDJ608)), *Y. pestis* (pBAD_{ssp}AYp), *V. cholerae* (pBAD_{ssp}AVc), and *P. aeruginosa* (pBAD_{ssp}APa) were expressed in the presence of 0.02% arabinose (8). The expression of plasmid-encoded *sspA* in the *sspA* mutant strain was confirmed by Western blot analysis using a polyclonal antibody against *E. coli* SspA.

Complementation of Phage P1 Growth on the *sspA* Mutant Strain—The assay was performed in two ways. In the first approach the growth of phage P1 was followed by looking at plaque formation on a solid plate, whereas in the second approach lytic growth was observed as cell lysis of a culture. The ability of the *E. coli* SspA mutants and the wild-type SspA from *E. coli*, *Y. pestis*, *V. cholerae*, and *P. aeruginosa* to complement phage P1 growth of the *sspA* mutant DJ6000 (68) was determined by expressing *sspA* *in trans* as described above in cells grown to the mid-log phase LB medium containing 20 mM CaCl₂, and when appropriate, 100 μ g/ml ampicillin. Strains were then infected with different dilutions of P1-vir (laboratory collection) for 20 min at room temperature. After 5 ml of 0.7% molten top agar containing 20 mM CaCl₂ were added, the cells were poured onto LB agar plates. The plates were incubated overnight at 37 °C, and the number of plaques and the plaque size were determined. The complementation test was carried out in at least three independent experiments for each strain.

The ability of the wild-type and mutant *E. coli* SspA to support lytic growth of the thermal-inducible prophage P1C_{mclr}.100 (37) in the *sspA* mutant DJ6000 (68) was determined by growing cells in LB medium at 30 °C to an A₆₀₀ value of 0.4 prior to induction of the prophage to lytic growth by a temperature shift to 42 °C. Lytic growth of phage P1 was determined by optically measuring the degree of cell lysis at 600 nm every 10 min after prophage induction. The wild-type and mutant *E. coli* SspA were expressed *in trans* in the absence of the inducer IPTG.

In Vitro Transcription—*In vitro* transcription of the P1 late promoter Ps was performed as described (8). The DNA template pHAL66 (2 nM) (8) encoding Ps was incubated at room temperature for 10 min with *E. coli* RNAP, Lpa (800 nM), and SspA (200 nM *E. coli* SspA; 400 nM *Y. pestis*, *V. cholerae*, and *P. aeruginosa* SspA in transcription buffer (300 mM potassium glutamate, 40 mM Tris-glutamate, 50 mM Mg-glutamate, 5 mM dithiothreitol, and 0.1 mg ml⁻¹ bovine serum albumin). The transcription reaction was initiated by the addition of NTPs (0.2 mM of ATP, GTP, and CTP; 0.02 mM for UTP including ~0.25 μ Ci of [α -³²P]UTP with the specific activity 3000 Ci/mM). The reactions were stopped after 10 min by addition of 5 μ l of stop solution (0.25 M EDTA, 50% glycerol, 0.25% (w/v) bromphenol blue, and 0.25% (w/v) xylene cyanol). The transcription products were denatured at 90 °C for 2 min and resolved on an 8% denaturing acrylamide gel. Proteins used in the transcription reactions were purified as previously described: RNAP holoenzyme (38), *E. coli* SspA (8), *Y. pestis*, *V. cholerae*, and *P. aeruginosa* SspA (18).

RESULTS

Crystal Structure of *Y. pestis* SspA—The SspA protein assumes the fold of the cytosolic GST (39) (Fig. 1 and Table II), which is in agreement with the observation that SspA displays sequence similarity with GST family members (40, 41). GST, a phase II detoxification enzyme, is functional as a dimer (42). The enzyme is present in all eukaryotes and several bacteria.

TABLE II
Secondary structural elements of SspA, GST B1-1, Ure2p, GST S1-1, and HPGDS

GST ^a	Mol A ^b	Mol B	GST B1-1 ^c	Ure2p ^d	GST S1-1 ^e	HPGDS ^f
	3 ₁₀ : 5–7			α: 100–107		
β1	11–15	11–15	2–5	114–118	3–7	4–9
α1	20–32	20–32	12–20	123–134	15–22	16–24
β2	36–40	37–40	26–31	139–143	29–32	29–34
α2	48–53	3 ₁₀ : 48–50	β: 36–37	3 ₁₀ : 150–152	3 ₁₀ : 38–41	3 ₁₀ : 39–42
β3	61–64	61–64	54–56	167–170	52–55	53–56
β4	67–70	67–70	62–64	176–178	58–60	59–62
α3	72–82	72–82	66–76	181–196	63–74	64–71
			3 ₁₀ : 77–80			3 ₁₀ : 76–78
α4	93–119	93–119	90–113	206–235	81–105	82–99
α5	122–138	122–138	122–139	242–273	112–136	109–135
	3 ₁₀ : 142–145	α: 141–145		α: 279–284		
α6	156–171	156–171	153–168	308–323	151–166	148–163
				3 ₁₀ : 327–330	3 ₁₀ : 168–171	
α7	180–191	180–191	176–186	332–342	175–186	172–183
α8	194–199	194–199	189–197	345–352	188–196	185–193
	3 ₁₀ : 202–205	3 ₁₀ : 202–205				

^a The secondary structural elements common for most cytosolic GSTs.

^b SspA.

^c PDB code 1A0F, Ref. 54.

^d PDB code 1G6W, Ref. 51.

^e PDB code 1GSQ, Ref. 53.

^f PDB code 1PD2, Ref. 45.

To date, at least thirteen distinct classes of cytosolic GST isozymes have been characterized, including alpha, beta, delta, kappa, lambda, mu, omega, phi, pi, sigma, theta, tau, and zeta, (43, 44). Most GST family members are catalytically active toward CDNB. However, proteins that adopt a GST fold but lack this activity, such as hematopoietic prostaglandin D synthase (HPGDS) (45), the cephalopod major lens protein S-crystallin (46–49), and the globular region of the yeast prion Ure2p (50–52), have also been identified. HPGDS and S-crystallin are similar to sigma-class GST subunit type 1 (GST S1-1) (PDB code 1GSQ, Ref. 53), whereas Ure2p and SspA (this work) are similar to beta-class GST subunit type 1 (GST B1-1) (PDB code 1A0F, Ref. 54). Detailed secondary structural element assignments for the above-mentioned GSTs and GST-like proteins can be found in Table II.

Two molecules of *Y. pestis* SspA, Mol A and Mol B, exist in the asymmetric unit as a dimer (Fig. 1). The two subunits are related by a 2-fold axis. Each subunit is composed of two domains, a small N-terminal 3-layer $\alpha\beta\alpha$ sandwich and a large C-terminal up-down helix bundle. The sandwich is centered by a 4-stranded β -sheet flanked by three helices in the order $\beta1-\alpha1-\beta2-\alpha2/3_{10}-\beta3-\beta4-\alpha3$. Two α -helices, $\alpha1$ and $\alpha3$, are located on one side of the β -sheet, whereas on the other side exists an α -helix ($\alpha2$) in Mol A, but a 3_{10} helix in Mol B (Fig. 1 and Table II). It should be noted that three and nine residues at the N termini of Mol A and Mol B, respectively, are absent in the structure. The superposition of Mol A and Mol B indicates that the conformation of the N-terminal domain is significantly different in the two molecules inasmuch as $\alpha2$ in Mol A is replaced by a 3_{10} helix in Mol B (Fig. 2A). It appears that the $\alpha2$ helix exists also as either a β -strand or a 3_{10} helix in different GSTs and GST-like proteins (Fig. 2 and Table II). The C-terminal domain of *Y. pestis* SspA consists of five α -helices, $\alpha4$ through $\alpha8$, and two 3_{10} helices, located at the C-terminal end of $\alpha5$ and $\alpha8$, respectively (Fig. 1). All five α -helices are present in cytosolic GSTs and GST-like proteins (Fig. 2 and Table II).

SspA Is Impaired in GST Activity and Binding of GSH—To determine whether SspA has GST activity, we measured the ability of SspA to catalyze the addition of the tripeptide thiol GSH to electrophilic functional groups in endogenous and xenobiotic substrates exemplified by CDNB (42). A positive control, GST A1-1, could catalyze the reaction as expected;

whereas neither *Y. pestis* nor *E. coli* SspA could do so, behaving like *E. coli* RpoS, a negative control (Table III).

Structure-based sequence alignment indicated that the catalytic residue Cys¹⁰ of GST B1-1 is replaced with Phe²¹ and Tyr²¹ in *Y. pestis* and *E. coli* SspA, respectively (Table IV), which might account for the lack of GST activity. Nevertheless, *E. coli* SspA with Tyr²¹ replaced by a cysteine residue, SspAY21C, is still catalytically inactive toward CDNB (Table III), suggesting that the structure of SspA further differs from that of GST B1-1. Fig. 3 depicts the superposition of four GSH-binding sites, including that of GST B1-1 in complex with GSH (PDB code 2PMT, Ref. 55), Ure2p in complex with GSH (PDB code 1K0D, Ref. 56), *Y. pestis* SspA (this work), and an *E. coli* SspA model (this work). It is known that Ure2p binds GSH (56) because all protein-GSH interactions are conserved; however, Ure2p is inactive toward CDNB (50, 57, 58) because it lacks the catalytic Cys residue (Table IV and Fig. 3). In the putative GSH-binding site of SspA, two residues important for protein-GSH interactions are missing at positions 21 and 58 (Table IV). At position 21, residue Phe (*Y. pestis* SspA) or Tyr (*E. coli* SspA) can neither form a hydrogen bond with the -SH group of GSH, nor can they facilitate the GSH conjugation reaction with CDNB (Fig. 3). In addition, the bulky hydrophobic side chain of Phe or Tyr may cause a steric hindrance for the binding of GSH. At position 58, the side chains of residues Thr (*Y. pestis* SspA) and Ser (*E. coli* SspA), respectively, are shorter than that of the corresponding residues Gln in GST B1-1 and Arg in Ure2p (Table IV). Therefore, the residue at position 58 of SspA not only eliminates a hydrogen bond between the protein and GSH (Fig. 3), but also dramatically changes the shape of the GSH-binding site.

Taken together, we predicted that SspA does not bind GSH. Indeed, we attempted soaking either GSH or a GSH analog, S-hexyl-GSH, into the *Y. pestis* SspA crystal, but were not able to identify any bound ligands. Furthermore, SspA did not bind to a GSH-Sepharose matrix (data not shown). Thus, SspA assumes the GST fold but lacks any GST function that requires GSH as a cofactor.

Structural Indication of Functional Regions—The superposition of Mol A and Mol B of *Y. pestis* SspA reveals three flexible regions, the N and C termini and $\alpha2$ (Fig. 2A). The conformations of these three regions in SspA also differ significantly

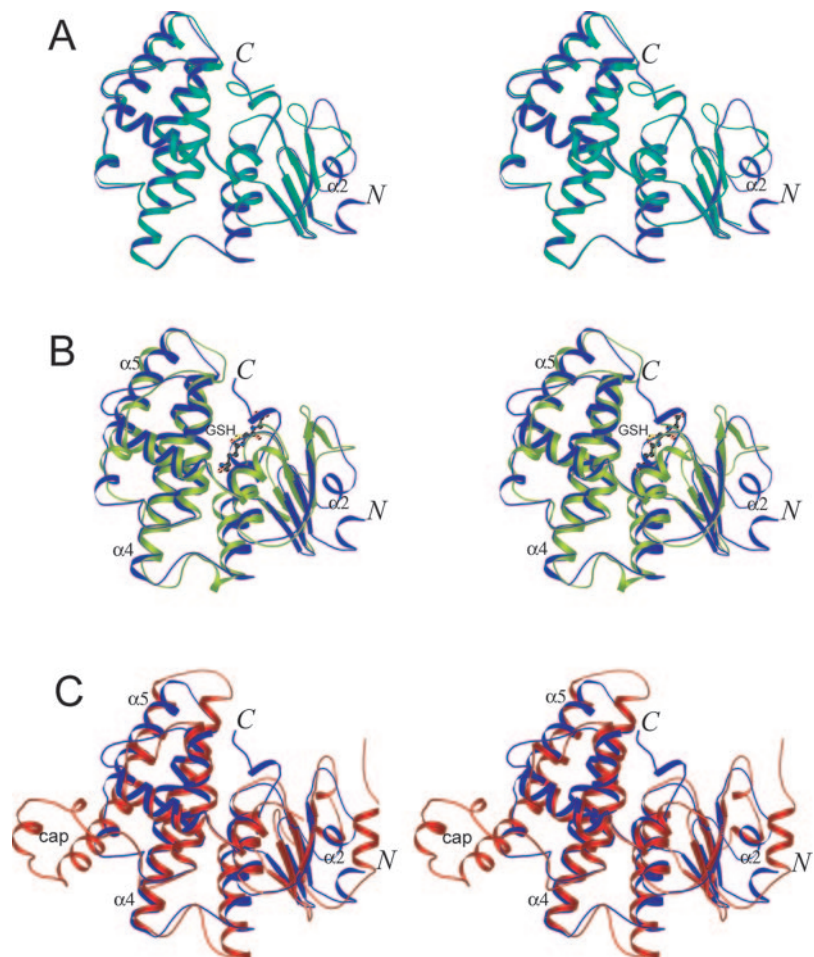


FIG. 2. Stereoviews showing structural comparisons. A, comparison between Mol A (blue) and Mol B (cyan) of *Y. pestis* SspA. B, comparison between Mol A of *Y. pestis* SspA (blue, this work) and one subunit of GST B1-1 in complex with GSH (green, PDB code 2PMT, Ref. 55). C, comparison between Mol A of *Y. pestis* SspA (blue, this work) and Ure2p (red, PDB code 1G6W, Ref. 51). The protein is illustrated as ribbon diagrams (helices as spirals, β -strands as arrows, and loops as pipes). The figure was prepared with MOLSCRIPT (65).

TABLE III
GST activity measurement of *Y. pestis* SspA, *E. coli* SspA, RpoS, and GST A1-1

Protein	GST activity \pm S.D.
	$\mu\text{mol}^{-1} \text{min}^{-1} \text{mg protein}^{-1}$
GST A1-1	55 ± 5
RpoS	7 ± 2
<i>Y. pestis</i> SspA	8 ± 2
<i>E. coli</i> SspA	7 ± 1
<i>E. coli</i> SspAY21C	10 ± 1

from those in GST B1-1 (Fig. 2B) and Ure2p (Fig. 2C). In GSTs, the α 2- β 3 loop (Tables II and IV) is involved in GSH binding, and the C-terminal region is involved in the binding of xenobiotic substrates (39, 59). In Ure2p, although the α 2- β 3 loop is also involved in GSH binding as in GSTs (Tables II and IV), the N-terminal region modulates the capacity of Ure2p to assemble into prion filaments (56), and the α 2 and C-terminal regions act to inhibit the formation of prions (52). In addition, Ure2p has a 32-residue insertion that forms the flexible cap (Fig. 2C), a preferred region for protein-protein interactions, which is likely to be involved in the assembly of Ure2p into amyloid fibrils (51). Therefore, to understand the relationship between structure and function of SspA, the role of the three flexible regions needs to be elucidated.

A multiple sequence alignment of 50 SspA orthologs revealed a high degree of sequence similarity, with 20 residues strictly conserved (Fig. 4). Among the 20 residues, Pro⁶⁰, Leu⁶², Tyr⁷⁸, and Arg¹⁰⁰ are of structural importance for the GST fold (41), whereas Pro⁸⁴, His⁸⁵, Pro⁸⁶, and Leu⁸⁸, which are located in the loop region between helices α 3 and α 4, are specific to SspA. The

α 3- α 4 loop region (Fig. 1) is comprised of surface-exposed residues (Fig. 5, panels A and C). The side chains of these residues in the dimer form a surface pocket from which the rings of His⁸⁵ and Tyr⁹² of each subunit protrude (Fig. 5, panels B and D). The dimensions of the surface pocket are $\sim 23 \times 22 \times 10$ Å, and the residues forming the pocket are mainly hydrophobic, suggesting that it may serve as a site for protein-protein interactions. In addition, both His⁸⁵ and Tyr⁹² can act as hydrogen bond donors and thereby enhance the interactions between SspA and its partner protein.

Mutational Analysis of the Structural Basis for SspA Function—Modeling of *E. coli* SspA on the basis of the *Y. pestis* SspA structure resulted in a similar structure (The entire *E. coli* SspA model is not shown; The GSH-binding site of the *E. coli* SspA model is shown in Fig. 3). Since the function of *Y. pestis* SspA is unknown, we used *E. coli* SspA to study the structural basis for SspA function. The function of *E. coli* SspA was assayed for its two known functions: to confer acid resistance of *E. coli*; (68) and to support the lytic growth of phage P1 by activating transcription of phage P1 late genes (8, 9).

To test the functional importance of the flexible N and C termini of SspA, we deleted nine amino acid residues from each terminus, resulting in the deletion mutants SspA Δ 1-9 and SspA Δ 204-212, respectively. When supplied *in trans* from pBAD Δ sspA Δ 1-9 and pBAD Δ sspA Δ 204-212, the deletion mutants fully complemented acid resistance of the *sspA* *E. coli* mutant strain upon exposure to low pH, with survival rates comparable to wild-type SspA, and they supported phage P1 growth (data not shown), indicating that the N and C termini are not required for SspA function. We did not pursue structural perturbation of the α 2 region as it is implicated for GSH

TABLE IV
Major GSH-interacting residues in GST B1-1, Ure2p, *Y. pestis* SspA, and *E. coli* SspA

	GST B1-1	Ure2p	<i>Y. pestis</i> SspA	<i>E. coli</i> SspA
Catalytic residue	Cys ¹⁰	Asn ¹²⁴	Phe ²¹	Tyr ²¹
VDW and H-bonding	Gln ⁵¹	Arg ¹⁶⁴	Thr ⁵⁸	Ser ⁵⁸
H-bonding	Val ⁵²	Val ¹⁶⁵	Val ⁵⁹	Val ⁵⁹
Cis-conformation	Pro ⁵³	Pro ¹⁶⁶	Pro ⁶⁰	Pro ⁶⁰
Unusual ϕ/ψ angles	Glu ⁶⁵	Glu ¹⁸⁰	Glu ⁷¹	Glu ⁷¹
Amide H-bonding	Gly ⁶⁶	Ser ¹⁸¹	Ser ⁷²	Ser ⁷²

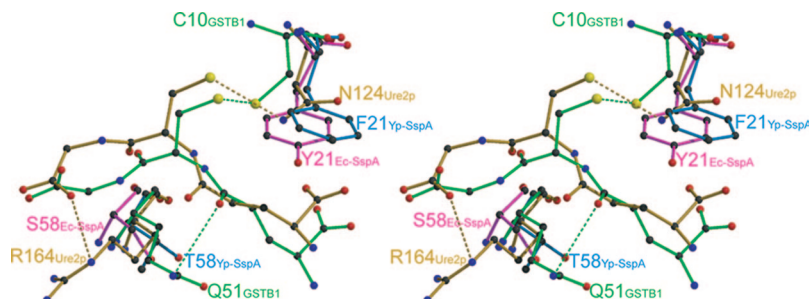


FIG. 3. **GSH-binding site of GST and GST-like proteins.** Stereoview showing the superposition of the GSH-binding site in GST B1-1 (green, PDB code 2PMT, Ref. 55), Ure2p (orange, PDB code 1K0D, Ref. 56), *Y. pestis* SspA (blue, this work), and *E. coli* SspA model (purple, this work). Amino acid residues and GSH are illustrated as ball-and-stick models in atomic color scheme (carbon in black, nitrogen in blue, oxygen in red, and sulfur in yellow). Dotted lines indicate functionally significant hydrogen bonds. This figure was prepared with MOLSCRIPT (65) and Raster3D (66).

binding in GST and Ure2p and for prion activity in Ure2p.

To assess the functional importance of the surface-exposed pocket, we made single alanine substitutions of residues Arg⁸², Pro⁸⁴, His⁸⁵, Pro⁸⁶, and Tyr⁹², a double alanine substitution H85A/Y92A, and a triple alanine substitution P84A/H85A/P86A. The ability of each of these alanine-substituted mutants to complement acid-resistance of *E. coli* and support phage P1 growth, when expressed *in trans* from plasmids in an *sspA* background, was determined (Fig. 6A). Whereas the wild-type strain was acid-resistant, and the *sspA* mutant was acid-sensitive, the wild-type SspA protein provided *in trans* conferred acid tolerance of the *sspA* mutant as described (68) (Fig. 6A, columns 1–3). Among the single alanine substitution SspA mutants, the mutant P84A behaved almost like wild-type SspA (Fig. 6A, compare columns 3 and 5), whereas the ability of mutants R82A, H85A, P86A, and Y92A to support acid resistance was reduced 4–8-fold compared with the wild type (Fig. 6A, compare columns 4, 6–8 with column 3). Interestingly, whereas elimination of the ring structure of either His⁸⁵ or Tyr⁹² decreased the complementation of acid resistance 8-fold, substitution of both His⁸⁵ and Tyr⁹² with alanine (H85A/Y92A) reduced SspA activity about 40-fold (Fig. 6A, column 9), suggesting a cooperative action by residues His⁸⁵ and Tyr⁹² in the SspA function. Furthermore, the triple substitution that replaced SspA residues Pro⁸⁴, His⁸⁵, and Pro⁸⁶ with alanine (P84A/H85A/P86A) almost abolished SspA complementation of acid resistance (Fig. 6A, column 10), indicating that the overall structure of the pocket, in addition to the ring systems of His⁸⁵ and Tyr⁹², is important for SspA function.

To determine whether *sspA* encoding the triple mutant SspAP84A/H85A/P86A is dominant over wild-type *sspA*, we determined the acid tolerance of the wild-type *sspA* background expressing the triple mutant SspA *in trans*. Apparently the triple mutant *sspA* gene is dominant over the wild-type allele as wild-type cells became partially acid sensitive (survival rate of 17% compared with 80% for the wild type), when expressing SspA/P84A/H85A/P86A *in trans* (Fig. 6A, column 11). This result is consistent with the notion that SspA functions as a dimer of which the surface-exposed pocket is formed by residues from both subunits (Fig. 5).

In addition, we examined the ability of these alanine-substituted SspA proteins to support the lytic growth of phage P1 in

a *sspA* mutant strain (Table V). In this assay, the lytic development of phage P1 was examined as the ability of P1-vir to form plaques on a *sspA* background expressing mutant SspA. A P1-vir phage was used because it forms clear plaques on a lawn of wild-type cells. Overall, the phenotype of the SspA alanine mutants with respect to phage P1 growth was less severe than that of acid resistance. For instance, although the triple mutation P84A/H85A/P86A abolished the ability of the *sspA* mutant to confer acid resistance, it was still in part able to support P1 growth. However, the plaques of phage P1 grown on the *sspA* mutant strain expressing SspA/P84A/H85A/P86A appeared turbid and were only about one-fourth of the wild type in size, indicating that the triple mutant supports the growth of phage P1 inefficiently. Other SspA mutants either affected P1 growth less significantly (P86A, Y92A, and H85A/Y92A) or behaved like the wild type in phage P1 plaque formation (R82A, P84A, and H85A).

To further analyze the effects of these *sspA* mutations on the growth of phage P1, we performed a kinetic assay of phage growth (Fig. 6B), which is more sensitive compared with the assay described above. In this assay, the ability of the thermal-inducible P1 prophage P1Cmclr.100 (37) to undergo lytic growth in a *sspA* background expressing mutant SspA was determined by optically measuring the degree of cell lysis (Fig. 6B). Under the conditions used, phage P1 completed a life cycle in the wild-type strain 30–40 min after thermal induction of the prophage to lytic growth, leading to cell lysis as reported (60). Similarly, it took phage P1 30–40 min after prophage induction to undergo lytic growth in the *sspA* mutant expressing either wild-type SspA, SspAR82A, SspAP84A, SspAH85A, or SspAP86A *in trans* (Fig. 6B), whereas the *sspA* mutant harboring a vector did not lyse even during prolonged incubation as previously reported (9). Though, the degree of cell lysis of the *sspA* background expressing the mutants P84A and P86A appeared less efficient compared with that of the wild type. However, the SspA mutants Y92A, H85A/Y92A, and P84A/H85A/P86A were defective in supporting lytic growth of phage P1 in the *sspA* mutant as cell lysis was delayed. Cell lysis of the *sspA* mutant expressing Y92A appeared 40–50 min after prophage induction, whereas cell lysis was further delayed 10 min in strains expressing SspAH85A/Y92A or SspAP84A/H85A/P86A. The growth assay allowed distinction between the

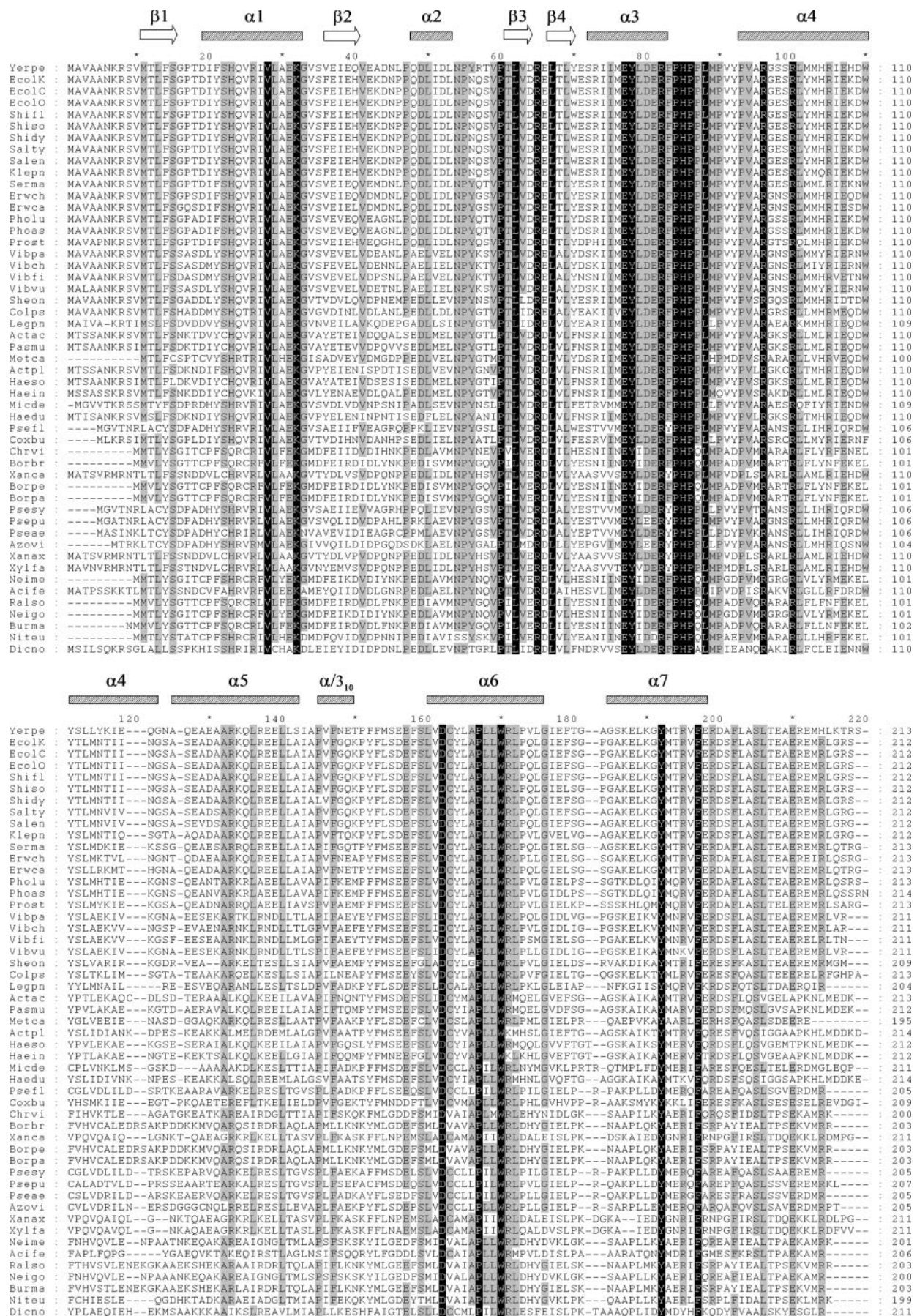


Fig. 4. Multiple sequence alignment of 50 SspA orthologs. Residues strictly conserved or chemically similar in at least 80% of the sequences are shown on black and gray backgrounds, respectively. Secondary structure elements shown above the alignment are in accordance to the structure of *Y. pestis* SspA (Table II). Species abbreviations: *Acfi*, *Acidithiobacillus ferrooxidans*; *Acta*, *Actinobacillus actinomycetemcomitans*;

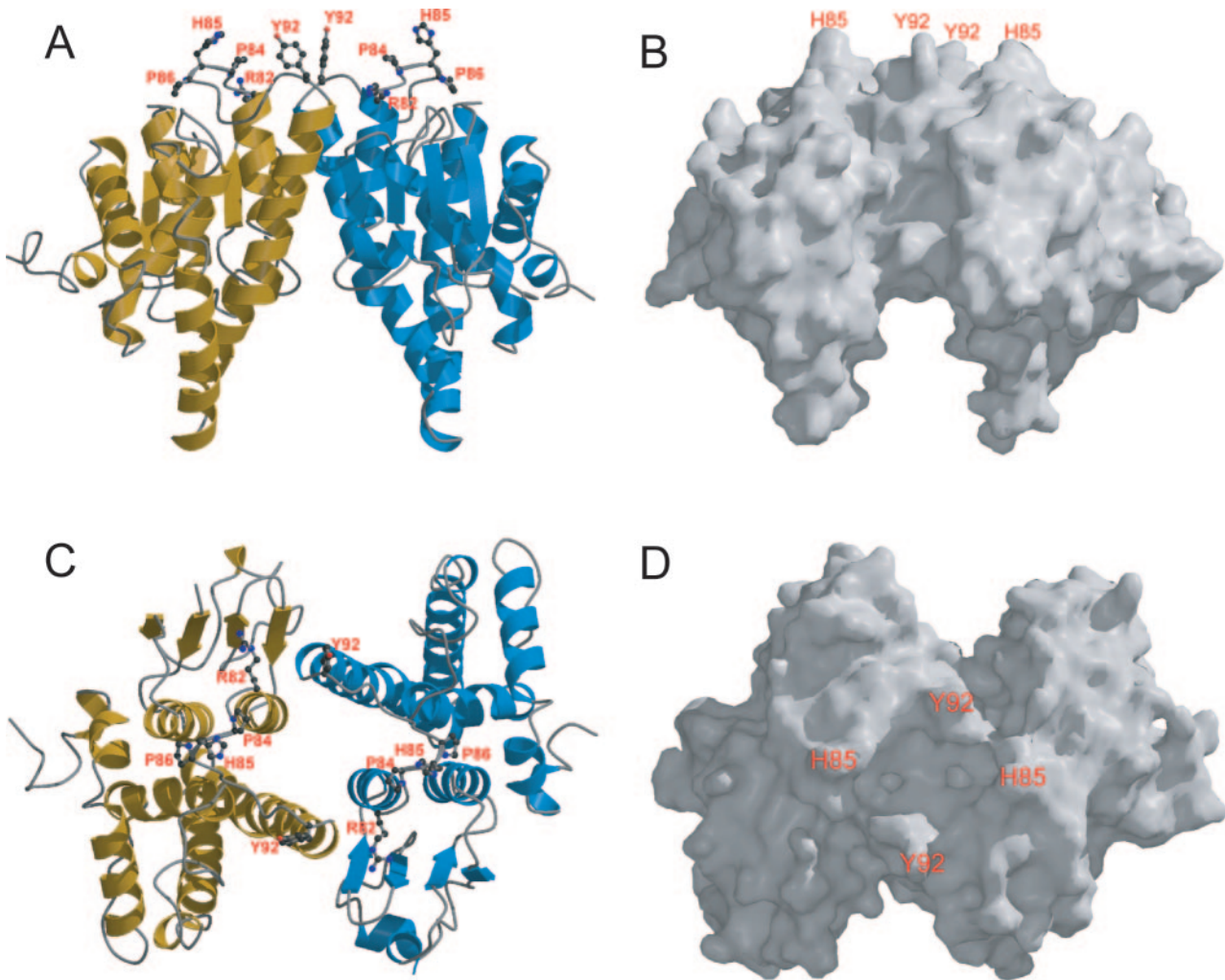


FIG. 5. **Functionally important pocket on the surface of dimeric *Y. pestis* SspA.** A and B, side views showing the edge of the pocket. C and D, top views showing the bottom of the pocket. In panels A and C, the protein is illustrated as ribbon diagrams (helices as spirals, β -strands as arrows, and loops as pipes) with the two subunits colored in cyan and orange, respectively. The side chains of pocket-defining residues are shown as ball-and-stick models in atomic color scheme (carbon in black, nitrogen in blue, and oxygen in red). In panels B and D, the pocket is visualized with space-filling models. The figure was prepared with MOLSCRIPT (65), Raster3D (66), and GRASP (67).

P1 growth phenotypes of the *sspA* mutant expressing the mutants H85A/Y92A and P84A/H85A/P86A. Cells expressing the H85A/Y92A mutant eventually lysed with a rate comparable with that of the cells expressing Y92A. The most severe effect on phage growth was observed for the SspA triple mutant P84A/H85A/P86A, which only displayed a minor degree of lysis compared with the strains encoding other SspA mutants.

To confirm that the defect of the SspA triple mutant in supporting the lytic growth of phage P1 is caused by its inability to activate transcription from the phage P1 late promoter, we performed *in vitro* transcription of the late promoter Ps using purified proteins (Fig. 6C). Indeed, whereas wild-type SspA and the phage-encoded factor Lpa-activated transcription of the P1 late promoter as previously reported (8), SspA84A/

H85A/P86A showed a 2–3-fold decrease in transcriptional activity compared with wild-type SspA (Fig. 6C), indicating that the surface-exposed pocket is involved in transcription activation by SspA. The residual transcription activity of the triple mutant SspA could account for the weak complementation of phage P1 growth on a *sspA* mutant by SspAP84A/H85A/P86A (Table V). Taken together, residues of the surface pocket, especially residues Pro⁸⁴, His⁸⁵, and Pro⁸⁶, are important for the ability of SspA to support the lytic growth of phage P1.

SspA orthologs from *Y. pestis*, *V. cholerae*, and *P. aeruginosa* are functional in *E. coli*—SspA is highly conserved among Gram-negative bacteria as shown in the multiple sequence alignment (Fig. 4). The 50 SspA orthologs included in the alignment display 40–100% sequence identity to SspA from

Actpl, *Actinobacillus pleuropneumoniae*; Azovi, *Azotobacter vinelandii*; Borbr, *Bordetella bronchiseptica*; Borpa, *Bordetella parapertussis*; Borpe, *Bordetella pertussis*; Burma, *Burkholderia mallei*; Chrvi, *Chromobacterium violaceum*; Colps, *Colwellia psychrerythraea* 34H; Coxbu, *Coxiella burnetii*; Dicno, *Dichelobacter nodosus*; EcolK, *E. coli* K-12; EcolC, *E. coli* CFT073; EcolO, *E. coli* O157:H7; Erwca, *Erwinia carotovora*; Erwch, *Erwinia chrysanthemi*; Haedu, *Haemophilus ducreyi*; Haein, *Haemophilus influenzae*; Haeso, *Haemophilus somnus*; Klepn, *Klebsiella pneumoniae*; Legpn, *Legionella pneumophila*; Metca, *Methylococcus capsulatus*; Micde, *Microbulbifer degradans*; Neigo, *Neisseria gonorrhoeae*; Neime, *Neisseria meningitidis*; Niteu, *Nitrosomonas europaea*; Pasmu, *Pasteurella multocida*; Phoas, *Photobacterium symbiotica*; Pholu, *Photobacterium luminescens*; Prost, *Providencia stuartii*; Pseae, *P. aeruginosa*; Psefl, *Pseudomonas fluorescens*; Psepu, *Pseudomonas putida*; Psesy, *Pseudomonas syringae*; Ralso, *Ralstonia solanacearum*; Salen, *Salmonella enterica*; Salty, *Salmonella typhimurium* LT2; Serma, *Serratia marcescens*; Sheon, *Shewanella oneidensis*; Shidy, *Shigella dysenteriae*; Shifl, *Shigella flexneri*; Shiso, *Shigella sonnei*; Vibch, *V. cholerae*; Vibfi, *Vibrio fischeri*; Vibpa, *Vibrio parahaemolyticus*; Vibvu, *Vibrio vulnificus*; Xanax, *Xanthomonas axonopodis*; Xanca, *Xanthomonas campestris*; Xylfa, *Xylella fastidiosa*; and Yerpe, *Y. pestis*.

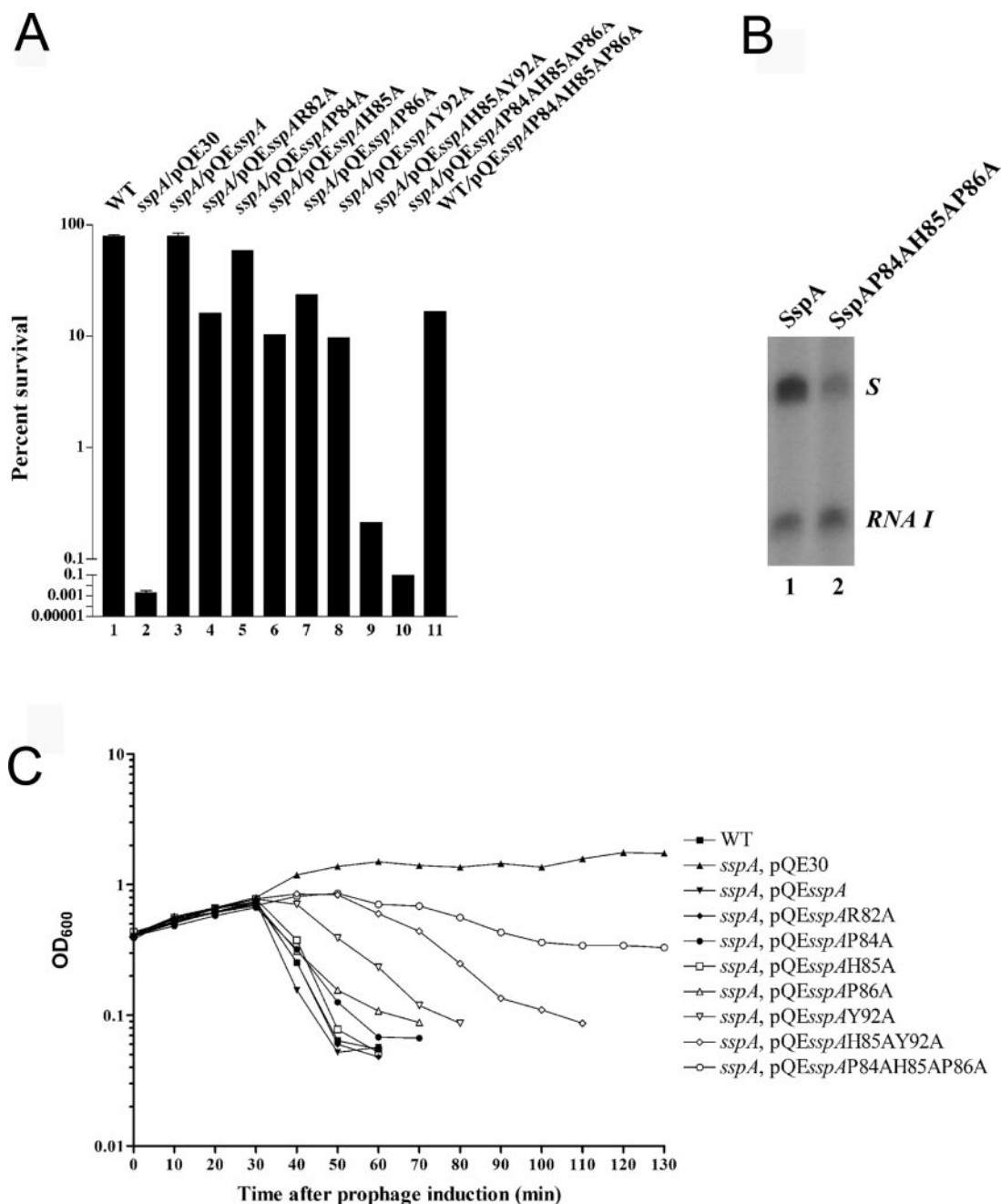


FIG. 6. The surface pocket is important for *E. coli* SspA activity. *A*, acid tolerance test of the *sspA* mutant strain expressing different mutant SspA proteins, which are altered in the surface pocket. The acid resistance assay was carried out as described under “Experimental Procedures.” The following strains were assayed: wild-type MG1655 (column 1), the *sspA* mutant harboring the vector pQE30 (column 2), the *sspA* mutant expressing wild-type SspA (pQE*sspA*, column 3), SspAR82A (pQE*sspA*R82A, column 4), SspAP84A (pQE*sspA*P84A, column 5), SspAH85A (pQE*sspA*H85A, column 6), SspAP86A (pQE*sspA*P86A, column 7), SspAY92A (pQE*sspA*Y92A, column 8), SspAH85A/Y92A (pQE*sspA*H85A/Y92A, column 9), and SspAP84A/H85A/P86A (pQE*sspA*P84A/H85A/P86A, column 10), respectively. The complementation test of the *sspA* triple mutation (pQE*sspA*P84A/H85A/P86A) in the wild-type MG1655 background is shown in column 11. Error bars represent S.D. of at least three independent experiments. *B*, lytic growth of phage P1 in a *sspA* background expressing wild-type and mutant SspA *in trans*. Strains carrying the thermal-inducible prophage P1Cmclr.100 were grown at 30 °C to $A_{600} \sim 0.4$, then lytic growth of P1Cmclr.100 was induced by shifting the cultures to 42 °C as described under “Experimental Procedures.” Lytic growth of phage P1 leading to cell lysis was determined by measuring cell density at 600 nm upon prophage induction. *C*, transcriptional activation of the phage P1 late promoter *P_s* *in vitro* by wild-type and mutant SspA. As described under “Experimental Procedures,” *in vitro* transcription by *E. coli* RNAP was carried out in the presence of Lpa and either wild-type *E. coli* SspA (lane 1) or the SspA triple mutant (SspAP84A/H85A/P86A, lane 2). The transcripts from the P1 late promoter (*S*) and the control transcript *RNA I* are indicated.

E. coli K-12. The high level of sequence identity indicates that the SspA orthologs share the same tertiary structure, and thus are likely to have a similar function. In this work, we studied the function of *Y. pestis*, *V. cholerae*, and *P. aeruginosa* SspA in *E. coli*. The amino acid sequences of SspA proteins from *Y. pestis*, *V. cholerae*, and *P. aeruginosa* are 83, 72, and 53% identical, and 90, 86, and 70% similar to *E. coli* SspA, respec-

tively (18). To test whether *Y. pestis*, *V. cholerae*, and *P. aeruginosa* SspA are functional in *E. coli*, we examined the ability of these SspA orthologs to confer acid resistance and to support propagation of phage P1 in the *sspA* mutant as described above. The three SspA orthologs were expressed *in trans* from the plasmids pBAD*sspAYp*, pBAD*sspAVc*, and pBAD*sspAPa*, and *E. coli* SspA was from pBAD*sspAEc*.

Apparently, SspA from *Y. pestis*, *V. cholerae*, and *P. aeruginosa* converts the acid-sensitive *sspA* phenotype to acid-resistant (Fig. 7A, columns 4–6), indicating that these SspA orthologs are functionally complementary in supporting acid resistance of *E. coli*. However, the ability of these SspA orthologs to support the lytic growth of phage P1 differ (Table V). As expected, phage P1 did not grow in the *sspA* mutant harboring the *sspA* cloning vector pBAD24, while *E. coli* SspA fully supports the lytic growth of phage P1 in the *sspA* mutant. Interestingly, *Y. pestis* SspA was the only SspA ortholog tested, in addition to *E. coli* SspA, which supported the propagation of phage P1, but with reduced ability; the phage plaque appeared turbid, and the plaque size was about one-fourth of the size observed for *E. coli* SspA. Consistent with the P1 growth complementation test, *in vitro* transcription of the P1 late promoter *P_s* by SspA and Lpa revealed that the *E. coli* and *Y. pestis* SspA proteins activate transcription (Fig. 7B, lanes 1 and 2), whereas SspA from *V. cholerae* and *P. aeruginosa* were unable to activate transcription (Fig. 7B, lanes 3 and 4). In

addition, *Y. pestis* SspA activated P1 late transcription 4-fold less efficient compared with *E. coli* SspA.

DISCUSSION

The crystal structure of the *Y. pestis* SspA protein, determined at 2.0-Å resolution, reveals a GST fold (Figs. 1 and 2). The GST fold of SspA is similar to that of the yeast prion protein Ure2p. However, SspA does not bind GSH, nor does it have GST activity. In contrast, Ure2p binds GSH, although it does not have GST activity. The structure of *E. coli* SspA was modeled on the basis of the structure of *Y. pestis* SspA. The two SspA orthologs are expected to have very similar three-dimensional structures because of the high degree of conservation in their amino acid sequences. We elucidated the structural basis for the SspA function using *E. coli* as a model system because the function of *Y. pestis* SspA currently is unknown, whereas *E. coli* SspA as an RNAP-associated protein is known to be important for transcriptional activation of the phage P1 late promoter and stationary phase-induced acid tolerance. Furthermore, we demonstrated that the SspA orthologs from *Y. pestis*, *V. cholerae*, and *P. aeruginosa* are all fully functional in supporting the acid resistance of *E. coli* but behave differently in supporting the lytic growth of phage P1.

Structural Basis for the SspA Function—SspA consists of two subunits Mol A and Mol B (Fig. 1). In addition to the GST fold, a noticeable feature of the three-dimensional structure of SspA is a surface-exposed pocket, encompassed by the interface of the two subunits involving amino acid residues Arg⁸², Pro⁸⁴, His⁸⁵, Pro⁸⁶, and Tyr⁹² (Fig. 5). We have demonstrated that this pocket is important for SspA activity. Mutational analysis indicated that while single substitution of surface pocket residues has minimal or no effect on the ability of SspA to support the acid resistance of *E. coli* and the lytic growth of phage P1, the triple substitution P84A/H85A/P86A abolishes these activities. These results suggest that the overall structure of the surface pocket is important for SspA function. Thus, it is likely that the proline residues at positions 84 and 86 not only ensure correct positioning of the imidazole ring of His⁸⁵, but also participate in defining the overall structure of the pocket. The importance of the residue stretch Pro⁸⁴-His⁸⁵-Pro⁸⁶ is further reflected by its strict conservation among SspA orthologs (Fig.

TABLE V
Growth complementation of phage P1 in an *sspA* mutant background expressing mutant *E. coli* SspA and wild-type SspA from *E. coli*, *Y. pestis*, *V. cholerae*, and *P. aeruginosa*

Phage P1 growth as determined from the plaque size, where +++ indicates the plaque size of wild type, ++ indicates a plaque size between 50 and 75% of the wild-type plaque, and + indicates a plaque size of about 25% that of wild type.

Strain	Phage P1 growth ^a
Wild type	+++
<i>sspA</i> , pQE30	–
<i>sspA</i> , pQE <i>sspA</i>	+++
<i>sspA</i> , pQE <i>sspA</i> R82A	+++
<i>sspA</i> , pQE <i>sspA</i> P84A	+++
<i>sspA</i> , pQE <i>sspA</i> H85A	+++
<i>sspA</i> , pQE <i>sspA</i> P86A	++
<i>sspA</i> , pQE <i>sspA</i> Y92A	++
<i>sspA</i> , pQE <i>sspA</i> H85AY92A	+
<i>sspA</i> , pQE <i>sspA</i> P84AH85AP86A	–
<i>sspA</i> , pBAD24	–
<i>sspA</i> , pBAD <i>sspA</i> Ec	+++
<i>sspA</i> , pBAD <i>sspA</i> Yp	++
<i>SspA</i> , pBAD <i>sspA</i> Vc	–
<i>SspA</i> , pBAD <i>sspA</i> Pa	–

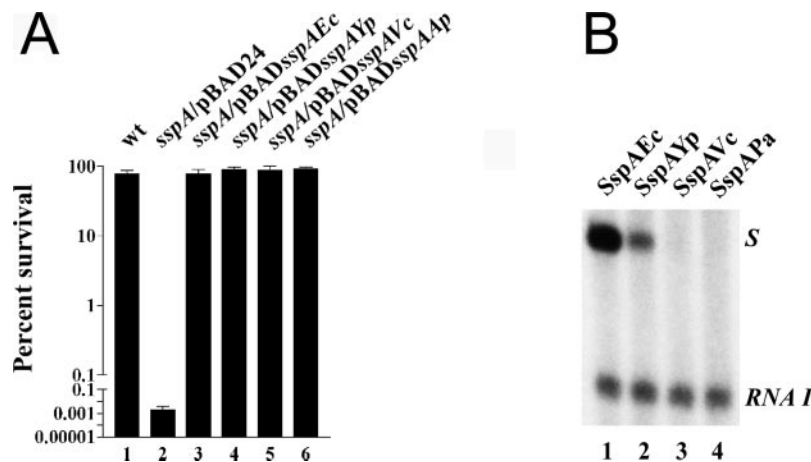


FIG. 7. **Functional complementarity of SspA orthologs.** SspA orthologs from *Y. pestis*, *V. cholerae*, and *P. aeruginosa* are fully functional in stationary phase-induced acid tolerance of *E. coli* but behave differently in supporting phage P1 lytic development. A, acid tolerance test of the *E. coli* *sspA* mutant strain expressing different SspA orthologs. The acid resistance assay was carried out as described under “Experimental Procedures.” The following strains were assayed: wild-type *E. coli* MG1655 (column 1), the *sspA* mutant containing the vector pBAD24 (column 2), and the *sspA* mutant expressing the *sspA* gene from *E. coli* (pBAD*sspA*Ec, column 3), *Y. pestis* (pBAD*sspA*Yp, column 4), *V. cholerae* (pBAD*sspA*Vc, column 5), and *P. aeruginosa* (pBAD*sspA*Pa, column 6), respectively. Error bars represent S.D. of at least three independent experiments. B, transcriptional activation of the phage P1 late promoter *P_s* by different SspA orthologs *in vitro*. As described under “Experimental Procedures,” *in vitro* transcription by *E. coli* RNAP was carried out in the presence of Lpa and either *E. coli* SspA (lane 1), *Y. pestis* SspA (lane 2), *V. cholerae* SspA (lane 3), or *P. aeruginosa* SspA (lane 4). The transcripts from the P1 late promoter (S) and the control transcript *RNA I* are indicated.

4). Since the structure of the surface pocket suggests that it is a region for potential protein-protein interactions and that it is important for SspA function in both *E. coli* and phage P1 late transcription, we speculate that the pocket serves as a binding site for RNAP. The effect of mutations in the surface pocket on the ability of SspA to complement phage P1 growth appeared less severe compared with the ability to support acid resistance (Table V and Fig. 6). This could be caused by the possibility that the phage-encoded co-activator Lpa stabilizes the SspA-RNAP interaction. In addition, the three-dimensional structure of SspA reveals the flexible N and C termini (Fig. 2). Unlike the N- and C-terminal regions of the GST-like Ure2p protein, which are functionally important (51, 61), deletions of the N and C termini of SspA do not affect SspA function.

Because the formation of the surface-exposed pocket, which is important for SspA activity, requires both Mol A and Mol B, SspA must function as a dimer. In support of this notion, we showed that the triple *sspA* mutation P84A/H85A/P86A exhibits a dominant negative phenotype in a wild-type background (Fig. 6A, compare columns 1 and 11). Note that residues that participate in the dimer formation of Ure2p are also important for transcription regulation (61), suggesting that Ure2p is also functional as a dimer. However, Ure2p does not contain a surface-exposed pocket like that of SspA. Instead, a cleft between the two subunits of Ure2p, which is next to the GSH-binding site, has been suggested to serve as the interaction site for proteins that bind to Ure2p (52). It remains to be elucidated whether the corresponding cleft in SspA is involved in the SspA function.

SspA Orthologs Are Functionally Complementary—SspA is highly conserved among Gram-negative bacteria. We have demonstrated that the SspA orthologs from *Y. pestis*, *V. cholerae*, and *P. aeruginosa* are fully functional in supporting acid resistance of *E. coli*, indicating that these SspA orthologs share a common function in the cell. However, only *Y. pestis* SspA could partially support the growth of phage P1 in *E. coli*. Consistent with this, *Y. pestis* SspA shares the highest degree of sequence conservation with *E. coli* SspA among the SspA orthologs tested. Thus, it is likely that phage P1 evolved to use SspA for its development in *E. coli*.

Therefore, SspA is most likely involved in acid tolerance of *Y. pestis*, *V. cholerae*, *P. aeruginosa*, and possibly other species encoding *sspA* as well. Acid tolerance is important for the ability of enteric bacteria such as *E. coli* O157:H7 to survive the low pH environment they encounter upon passage through the gastrointestinal tract during infection of the mammalian host (62–64). Since SspA is required for acid resistance (68), it most likely plays an important role in bacterial pathogenesis. The finding that the surface pocket residues Pro⁸⁴, His⁸⁵, and Pro⁸⁶, which are important for activity of *E. coli* SspA, are strictly conserved in 50 SspA orthologs (Fig. 4), suggests that the pocket is important for SspA function in general. Thus, this surface pocket provides a potential target for putative inhibitors of SspA function.

Acknowledgment—We thank Zbigniew Dauter for assistance during x-ray data acquisition.

REFERENCES

- Zhang, G., Campbell, E. A., Minakhin, L., Richter, C., Severinov, K., and Darst, S. A. (1999) *Cell* **98**, 811–824
- Vassilyev, D. G., Sekine, S., Laptenko, O., Lee, J., Vassilyeva, M. N., Borukhov, S., and Yokoyama, S. (2002) *Nature* **417**, 712–719
- Burgess, R. R., Erickson, B., Gentry, D. R., Gribskov, M., Hager, D., Lesley, S., Strickland, M., and Thompson, N. (1987) in *RNA Polymerase and the Regulation of Transcription* (Reznikoff, W. S., ed), pp. 3–15, Elsevier Science Publishing, New York
- Mooney, R. A., Artismovitch, I., and Landick, R. (1998) *J. Bacteriol.* **180**, 3265–3275
- von Hippel, P. H. (1998) *Science* **281**, 600–605
- Nudler, E., and Gottesman, M. E. (2002) *Genes Cells* **7**, 755–768
- Ishihama, A., and Saitoh, T. (1979) *J. Mol. Biol.* **129**, 517–530
- Hansen, A. M., Lehnher, H., Wang, X., Mobley, V., and Jin, D. J. (2003) *Mol. Microbiol.* **48**, 1621–1631
- Williams, M. D., Fuchs, J. A., and Flickinger, M. C. (1991) *Gene (Amst.)* **109**, 21–30
- Williams, M. D., Ouyang, T. X., and Flickinger, M. C. (1994) *Mol. Microbiol.* **11**, 1029–1043
- Atlung, T., and Ingmer, H. (1997) *Mol. Microbiol.* **24**, 7–17
- Hommais, F., Krin, E., Laurent-Winter, C., Soutourina, O., Malpertuy, A., Le Caer, J. P., Danchin, A., and Bertin, P. (2001) *Mol. Microbiol.* **40**, 20–36
- De Reuse, H., and Taha, M. K. (1997) *Res. Microbiol.* **148**, 289–303
- Baron, G. S., and Nano, F. E. (1998) *Mol. Microbiol.* **29**, 247–259
- Merrell, D. S., Hava, D. L., and Camilli, A. (2002) *Mol. Microbiol.* **43**, 1471–1491
- Xu, Q., Dziejman, M., and Mekalanos, J. J. (2003) *Proc. Natl. Acad. Sci. U. S. A.* **100**, 1286–1291
- Lauriano, C. M., Barker, J. R., Yoon, S. S., Nano, F. E., Arulanandam, B. P., Hassett, D. J., and Kloese, K. E. (2004) *Proc. Natl. Acad. Sci. U. S. A.* **101**, 4246–4249
- Andrykovitch, M., Routzahn, K. M., Li, M., Gu, Y., Waugh, D. S., and Ji, X. (2003) *Acta Crystallogr. Sect. D* **59**, 881–886
- Otwinowski, Z., and Minor, W. (1997) *Methods Enzymol.* **276**, 307–326
- Collaborative Computational Project Number 4. (1994) *Acta Crystallogr. Sect. D* **50**, 760–763
- Terwilliger, T. C., and Berendzen, J. (1999) *Acta Crystallogr. Sect. D* **55**, 849–861
- de La Fortelle, E., and Bricogne, G. (1997) *Methods Enzymol.* **276**, 472–494
- Cowtan, K. (1994) *Joint CCP4 and ESF-EACBM Newsletter on Protein Crystallography* **31**, 34–38
- Abrahams, J. P., and Leslie, A. G. W. (1996) *Acta Crystallogr. Sect. D* **52**, 30–42
- Lamzin, V. S., and Wilson, K. S. (1997) *Methods Enzymol.* **277**, 269–305
- Brünger, A. T., Adams, P. D., Clore, G. M., DeLano, W. L., Gros, P., Gross-Kunstleve, R. W., Jiang, J. S., Kuszewski, J., Nilges, M., Pannu, N. S., Read, R. J., Rice, L. M., Simonson, T., and Warren, G. L. (1998) *Acta Crystallogr. Sect. D* **54**, 905–921
- Jones, T. A., and Kjeldgaard, M. (1997) *Methods Enzymol.* **277**, 173–208
- Laskowski, R. A., MacArthur, M. W., Moss, D. S., and Thornton, J. M. (1993) *J. Appl. Crystallogr.* **26**, 283–291
- Powell, M. J. D. (1977) *Math. Prog.* **12**, 241–254
- Brünger, A. T., and Rice, L. M. (1997) *Methods Enzymol.* **277**, 243–269
- Engh, R. A., and Huber, R. (1991) *Acta Crystallogr. Sect. A* **47**, 392–400
- Thompson, J. D., Higgins, D. G., and Gibson, T. J. (1994) *Nucleic Acids Res.* **22**, 4673–4680
- Nicholas, K. B., Nicholas, H. B., Jr., and Deerfield, D. W. (1997) in *EMBNEWS* Vol. 4, p. 14
- Miller, J. H. (1972) *Experiments in Molecular Genetics*, Cold Spring Harbor Laboratory, Cold Spring Harbor, NY
- Sambrook, J., Fritsch, E. F., and Maniatis, T. (1989) *Molecular Cloning: A Laboratory Manual*, Cold Spring Harbor Laboratory Press, New York
- Guzman, L. M., Belin, D., Carson, M. J., and Beckwith, J. (1995) *J. Bacteriol.* **177**, 4121–4130
- Rosner, J. L. (1972) *Virology* **48**, 679–680
- Sukhodolets, M. V., and Jin, D. J. (1998) *J. Biol. Chem.* **273**, 7018–7023
- Dirr, H., Reinemer, P., and Huber, R. (1994) *Eur. J. Biochem.* **220**, 645–661
- Toung, Y. P., and Tu, C. P. (1992) *Biochem. Biophys. Res. Commun.* **182**, 355–360
- Rife, C. L., Parsons, J. F., Xiao, G., Gilliland, G. L., and Armstrong, R. N. (2003) *Proteins: Struct. Funct. Genet.* **53**, 777–782
- Hayes, J. D., and Pulford, D. J. (1995) *Crit. Rev. Biochem. Mol. Biol.* **30**, 445–600
- Sheehan, D., Meade, G., Foley, V. M., and Dowd, C. A. (2001) *Biochem. J.* **360**, 1–16
- Dixon, D. P., Laphorn, A., and Edwards, R. (2002) *Genome Biol* **3**, Reviews, 3004.1–10
- Kanaoka, Y., Ago, H., Inagaki, E., Nanayama, T., Miyano, M., Kikuno, R., Fujii, Y., Eguchi, N., Toh, H., Urade, Y., and Hayaishi, O. (1997) *Cell* **90**, 1085–1095
- Tomarev, S. I., and Zinovieva, R. D. (1988) *Nature* **336**, 86–88
- Tomarev, S. I., Zinovieva, R. D., and Piatigorsky, J. (1991) *J. Biol. Chem.* **266**, 24226–24231
- Tomarev, S. I., Chung, S., and Piatigorsky, J. (1995) *J. Mol. Evol.* **41**, 1048–1056
- Chuang, C. C., Wu, S. H., Chiou, S. H., and Chang, G. G. (1999) *Biophys. J.* **76**, 679–690
- Coschigano, P. W., and Magasanik, B. (1991) *Mol. Cell. Biol.* **11**, 822–832
- Bousset, L., Belrhali, H., Janin, J., Melki, R., and Morera, S. (2001) *Structure (Camb)* **9**, 39–46
- Umland, T. C., Taylor, K. L., Rhee, S., Wickner, R. B., and Davies, D. R. (2001) *Proc. Natl. Acad. Sci. U. S. A.* **98**, 1459–1464
- Ji, X., von Rosenvinge, E. C., Johnson, W. W., Tomarev, S. I., Piatigorsky, J., Armstrong, R. N., and Gilliland, G. L. (1995) *Biochemistry* **34**, 5317–5328
- Nishida, M., Harada, S., Noguchi, S., Satow, Y., Inoue, H., and Takahashi, K. (1998) *J. Mol. Biol.* **281**, 135–147
- Rosjohn, J., Polekhina, G., Feil, S. C., Allocati, N., Masulli, M., De Illio, C., and Parker, M. W. (1998) *Structure* **6**, 721–734
- Bousset, L., Belrhali, H., Melki, R., and Morera, S. (2001) *Biochemistry* **40**, 13564–13573
- Perrett, S., Freeman, S. J., Butler, P. J., and Fersht, A. R. (1999) *J. Mol. Biol.* **290**, 331–345
- Choi, J. H., Lou, W., and Vancura, A. (1998) *J. Biol. Chem.* **273**, 29915–29922
- Armstrong, R. N. (1997) *Chem. Res. Toxicol.* **10**, 2–18
- Yarmolinsky, M., and Sternberg, N. (1988) in *The Bacteriophages* (Calendar,

- R., ed) pp. 291–438, Plenum Press, New York
61. Kulkarni, A. A., Abul-Hamd, A. T., Rai, R., El Berry, H., and Cooper, T. G. (2001) *J. Biol. Chem.* **276**, 32136–32144
62. Lin, J., Lee, I. S., Frey, J., Slonczewski, J. L., and Foster, J. W. (1995) *J. Bacteriol.* **177**, 4097–4104
63. Bearson, S., Bearson, B., and Foster, J. W. (1997) *FEMS Microbiol. Lett.* **147**, 173–180
64. Merrell, D. S., and Camilli, A. (2002) *Curr. Opin. Microbiol.* **5**, 51–55
65. Kraulis, P. J. (1991) *J. Appl. Crystallogr.* **24**, 946–950
66. Merritt, E. A., and Bacon, D. J. (1997) *Methods Enzymol.* **277**, 505–524
67. Nicholls, A., Sharp, K. A., and Honig, B. (1991) *Proteins: Struct. Funct. Genet.* **11**, 281–296
68. Hansen, A., Qiu, Y., Yeh, N., Blattner, F. R., Durfee, T., and Jin, D. J. (2005) *Mol. Microbiol.* **56**, 713–734